ORIGINAL ARTICLE

Inhibition of gasdermin D-dependent pyroptosis attenuates the progression of silica-induced pulmonary inflammation and fibrosis

Meiyue Song [a,†], Jiaxin Wang [b,†], Youliang Sun [c], Junling Pang [a], Xiaona Li [a], Yuan Liu [d,e,f], Yitian Zhou [f,g], Peiran Yang [a], Tianhui Fan [a], Ying Liu [a], Zhaoguo Li [h], Xianmei Qi [a], Baicun Li [a], Xinri Zhang [i,*], Jing Wang [a,*], Chen Wang [a,d,e]

[a]State Key Laboratory of Medical Molecular Biology, Department of Physiology, Institute of Basic Medical Sciences Chinese Academy of Medical Sciences, School of Basic Medicine Peking Union Medical College, Beijing 100730, China
[b]Tsinghua-Peking Center for Life Sciences, Department of Biology, College of Medicine, Tsinghua University, Beijing 100084, China
[c]School of Pharmaceutical Sciences, Tsinghua University, Beijing 100084, China
[d]Department of Pulmonary and Critical Care Medicine, Center of Respiratory Medicine, China-Japan Friendship Hospital, Beijing 100029, China
[e]National Clinical Research Center for Respiratory Diseases, Beijing 100029, China
[f]Peking Union Medical College, Chinese Academy of Medical Sciences, Beijing 100730, China
[g]Peking Union Medical College, MD Program, Beijing 100730, China
[h]Department of Respiratory, the Second Affiliated Hospital of Harbin Medical University, Harbin 150086, China
[i]Department of Pulmonary and Critical Care Medicine, the First Hospital of Shanxi Medical University, Taiyuan 030001, China

Abstract   Silicosis is a leading cause of occupational disease-related morbidity and mortality worldwide, but the molecular basis underlying its development remains unclear. An accumulating body of evidence supports gasdermin D (GSDMD)-mediated pyroptosis as a key component in the development of

*Corresponding authors.

E-mail addresses: ykdzxr61@163.com (Xinri Zhang), wangjing@ibms.pumc.edu.cn (Jing Wang).

†These authors made equal contributions to this work.

various pulmonary diseases. However, there is little experimental evidence connecting silicosis and GSDMD-driven pyroptosis. In this work, we investigated the role of GSDMD-mediated pyroptosis in silicosis. Single-cell RNA sequencing of healthy and silicosis human and murine lung tissues indicated that GSDMD-induced pyroptosis in macrophages was relevant to silicosis progression. Through microscopy we then observed morphological alterations of pyroptosis in macrophages treated with silica. Measurement of interleukin-1β release, lactic dehydrogenase activity, and real-time propidium iodide staining further revealed that silica induced pyroptosis of macrophages. Additionally, we verified that both canonical (caspase-1-mediated) and non-canonical (caspase-4/5/11-mediated) signaling pathways mediated silica-induced pyroptosis activation, in vivo and in vitro. Notably, Gsdmd knockout mice exhibited dramatically alleviated silicosis phenotypes, which highlighted the pivotal role of pyroptosis in this disease. Taken together, our results demonstrated that macrophages underwent GSDMD-dependent pyroptosis in silicosis and inhibition of this process could serve as a viable clinical strategy for mitigating silicosis.

1. Introduction

Silicosis is a fibrotic lung disease caused by long-term inhalation of free crystalline silicon dioxide or silica[1]. Due to its high morbidity and mortality, silicosis is one of the most fatal occupational diseases worldwide[2,3]. Silicosis is characterized by diffuse interstitial pulmonary fibrosis and the formation of silicon nodules, which leads to impaired lung function or eventual respiratory failure and death[1]. Despite aggressive enforcement policies intended to lower the permissible occupational limits for respirable dust, millions of workers are still exposed to silica, especially in developing countries[4]. Exacerbating this issue, no effective drugs or other treatments have yet been developed, primarily due to a lack of understanding for the complex mechanisms underlying silicosis. In order to develop effective therapeutic strategies, research is therefore urgently needed to comprehensively clarify these mechanisms that drive silicosis progression.

It is widely accepted that macrophages, fibroblasts, and epithelial cells comprise the main effector cells of silicosis, all of which exert essential functions in the development of lung inflammation and fibrosis[4]. Among them, macrophages are the initiators of the silicosis-associated inflammatory signal cascades, as they are the first cells to encounter the inhaled silica particles via scavenger receptors (SRs) on the macrophage surface[5]. Phagocytosis of crystalline silica causes the alveolar macrophage to rupture and release cytotoxic oxidants, proteases, and inflammatory cytokines, especially interleukin (IL)-1β, into the extracellular space, which eventually result in diffuse alveolitis and subsequent fibrosis[4]. However, these events can be partially reversed through neutralization of IL-1β[6,7], suggesting that this cytokine likely performs essential roles in the pathogenesis of silicosis. Considering that IL-1β release is dependent on gasdermin D (GSDMD)-mediated pore formation[8–12], it is reasonable to speculate that GSDMD-induced pyroptosis also participates in the progression of silicosis.

Pyroptosis, which is largely elicited by GSDMD, features plasma membrane rupture, cellular swelling, and chromatin condensation[13,14]. GSDMD is composed of an N-terminal pore-forming domain and a C-terminal inhibitory domain, with a cleavage site targeted by caspase-1 or caspase-4/5/11[15]. As mentioned above, loss of membrane integrity and cell lysis

subsequently lead to a robust release of numerous cytokines and alarmins, which elicits an undue immune response and inflammation[16]. Accumulating evidence has shown that GSDMD-dependent pyroptosis drives an excessive inflammatory response and macrophage depletion in a variety of pulmonary diseases, in addition to exerting other unexpected effects[16], such as pulmonary fibrosis[17], asthma[18,19], acute respiratory distress syndrome (ARDS)[20,21], and others. Despite considerable attention and research, the relationship between GSDMD-driven pyroptosis and silicosis remains unclear. Thus, in this work, we investigated whether GSDMD-driven pyroptosis participates in the progression of silicosis.

To this end, we utilized single-cell RNA sequencing (scRNA-seq) to analyze GSDMD transcript levels in different lung tissue cells of human silicosis patients and a murine experimental model of silicosis. We found that pyroptosis-associated genes, including GSDMD, caspase-1, and caspase-4/5/11, were specifically overexpressed in macrophages of both human and murine silicosis lungs. We then verified the activation of GSDMD-induced pyroptosis and its canonical and non-canonical pathways during silicosis in vivo and in vitro through multiple lines of evidence. Additionally, Gsdmd knockout ($Gsdmd^{-/-}$) mice were protected against silicosis progression, suggesting that inhibition of pyroptosis may exert beneficial therapeutic effects on silicosis. These findings showed that silicosis macrophages indeed underwent GSDMD-induced pyroptosis and interrupting this process resulted in remarkable attenuation of silicosis. Taken together, this study provided a viable target for therapy of silicosis.

2. Materials and methods

2.1. Reagents

Crystalline silica (CAS7631-86-9; purity 99%) was obtained from Forsman Science Co., Ltd. (Beijing, China). The particles were baked at 180 °C for 2 h to remove endotoxins and water, then suspended in sterile phosphate buffered saline (PBS). The prepared silica suspension was sonicated for 20 min and vortexed for 30 s before use.

Specific caspase-1 inhibitor belnacasan (Beln; HY-13205) and caspase-11 inhibitor wedelolactone (Wede; HY-N0551) were

purchased from MCE Co., Ltd. (NJ, USA) and were dissolved in dimethyl sulfoxide (DMSO) to prepare stock solution of 10 mmol/L.

2.2. Human samples

Human lung tissue samples of silicosis were obtained from lung transplantation surgery patients ($n = 3$) with no history of lung disease of other etiology from China-Japan Friendship Hospital (Beijing, China). The control lung tissue sample was collected from the donor ($n = 3$). All included subjects provided written informed consent and all the procedures of this study were performed according to the Clinical Research Ethics Committee of the China-Japan Friendship Hospital (Beijing, China), which meets the ethical guidelines of the 1975 Declaration of Helsinki.

2.3. Animals

Gsdmd gene knockout C57BL/6J mice were generously presented by Feng Shao laboratory (National Institute of Biological Sciences, Beijing, China). All C57BL/6J mice were raised in specific pathogen free facilities under a 12 h light/dark cycle and standard rodent chow with controlled temperature (20−25 °C). All mice used in the experiments were male and approximately 8 weeks old. The Animal Protection and Use Committee of Peking Union Medical College (Beijing, China) approved all animal protocols in this study.

The silicosis model was established by intratracheal silica administration as previously described[22]. Briefly, 20 μL of silica suspended solution (600 mg silica were solute in 1 mL sterile PBS) was delivered into murine trachea after mice were anesthetized with 2% pentobarbital (i.p., 0.05 mL/10 g, Sigma−Aldrich, USA). The control counterparts underwent sham surgery and were administrated with an identical volume of PBS.

To investigate the essential role of pyroptosis involved in silicosis, we divided Gsdmd knockout mice into two groups, including PBS and silica groups (9 mice per group), and divided the wild type (WT) littermate into two groups, containing PBS and silica groups (9 mice per group). The modeling method is the same as above.

2.4. Cell culture

Murine peritoneal macrophages were obtained from peritoneal lavage fluid after administered with 3% thioglycolate by intraperitoneal injection for 72 h. The peritoneal macrophages were cultured in Dulbecco's modified Eagle medium (DMEM) supplemented with 10% fetal bovine serum (FBS) and 1% penicillin and streptomycin at 37 °C under 5% carbon dioxide. To observe the morphology alteration in macrophages treated with silica, we divided peritoneal macrophages into five groups, including PBS + vehicle, PBS + lipopolysaccharide (LPS, 50 ng/mL, L2630, Sigma−Aldrich), silica (50 μg/cm^2) + vehicle, silica + LPS, and LPS + nigericin (Nig, 20 μmol/L, MZ2157, Maokangbio, Carlsbad, CA, USA) groups. Peritoneal macrophages were treated with LPS for 3 h, subsequently stimulated by silica or Nig for another 3 h[23].

To investigate whether silica stimulation could elicit pyroptosis, peritoneal macrophages were divided into control group and silica-triggered group, in which continue to be divided into two identical parts by primed with or without LPS. Peritoneal macrophages were primed with LPS (50 ng/mL) for 3 h before administrated with silica (50 μg/cm^2). Cell supernatant was collected and then assayed after silica stimulation for 3 h, or at the indicated time.

Specific caspase-1 inhibitor Beln and caspase-11 inhibitor Wede were used to validate whether silica-induced pyroptosis was dependent on caspase-1 and/or caspase-11. For each inhibitor, primary peritoneal macrophages were randomly selected for 6 treatment groups: PBS + DMSO, PBS + high dose of inhibitor, silica + DMSO, and silica + low, moderate, or high dose of inhibitor, respectively. Primary macrophages were treated with different doses of Beln (5, 10, and 20 μmol/L) for 2 h and Wede (20, 40, and 80 μmol/L) for 30 min before silica stimulation for 3 h.

2.5. Single-cell RNA sequencing

The human scRNA-seq data was first processed using Cell Ranger software (version 4.0.0) to perform sequence alignment and get the feature-barcode matrices. For each sample, we discarded cells whose nFeature_RNA < 200. Genes that were expressed in less than 3 cells were also not included in further analysis. The scrublet software was used to remove the potential doublets from the datasets using default parameters. Then Seurat software was used to integrate samples and conduct unsupervised clustering. The clusters of cells were annotated with canonical cell type markers.

For mice, one sample from PBS control and one sample from silica models were integrated and clustered using Seurat R package (v3.1.2), approximately 31,767 single cells passed QC and annotated to 16 distinct clusters based on gene expression patterns of each cell. Cell Ranger (v3.1.0) software from 10×genomics and scrublet Python packages were hired to perform read alignment and quality control.

2.6. Lung function

Lung function was accessed by Buxco® Research Systems, Data Sciences International (St. Paul, MN, USA). After anesthesia, all mice were tracheostomized and inserted with a tracheal cannula connected with a computer-controlled ventilator. Under mechanical respiration, respiratory flow and airway pressure were measured to compute dynamic compliance (Cdyn) and airway resistance (RI). To measure the chord compliance (Cchord) and inspiratory capacity (IC), pressure−volume maneuvers were performed. Specially, Cchord was calculated from the related volumes and pressures where lungs slowly inhale with the pressure ranged between 0 and 10 cm H_2O. All indicators were evaluated based on the average from three duplicate values.

2.7. Histology

Human and murine lung tissue were fixed in 4% paraformaldehyde overnight. Samples were embedded in paraffin, and 5 μm sections were obtained for following staining. Hematoxylin and eosin (HE) staining was applied to quantitatively verify the state of inflammation according to Szapiel's method which consists of no inflammation (grade 0), mild (grade 1+), moderate (grade 2+), and severe (grade 3+). The inflammation score was based on the average of the scores of two persons familiar with pathology reading[24]. Masson's trichrome staining was used to evaluate the Fibrotic lesion Scores according to King's method[25]. The calculation of Fibrotic lesion Scores were determined as previously described[22]. In detail, different silicotic nodules were

first evaluated the fibrotic extent based on King's method, whose levels were ranging from 0 to 5. Then, every silicotic nodule got corresponding Fibrotic lesion Scores calculated as the fibrotic level score (0−5) multiplied by its percentage of area (over the whole sample). Finally, the sum of all nodules' scores was Fibrotic lesion score of each sample. All histological sections were visualized with 3D HISTECH digital scanner (Hungary). For immunohistochemistry (IHC), human and murine lung sections were stained with the anti-GSDMD antibody (1/200 dilution) at 4 °C overnight, then washed and incubated with secondary antibody for 1 h at room temperature. Positive stained area was blindly determined by two pathologists and reported as percentage. For immunofluorescent staining (IF), human and murine lung sections were blocked for 30 min in 5% fetal goat serum and subsequently incubated with anti-GSDMD (1/200 dilution) and anti-CD68 (1/500 dilution) at 4 °C overnight, and counterstained with secondary antibodies (Alexa Fluor® 488 for CD68 and AlexaFluor® 594 for GSDMD, respectively) for 1 h at room temperature. Nuclear was labeled with 4′,6-diamidino-2-phenylindole (DAPI). For murine lung sections, we also colocalized GSDMD with surfactant associated protein C (SP-C) (1/200 dilution) and α-smooth muscle actin (α-SMA; 1/200 dilution), respectively.

2.8. Right ventricular systolic pressure (RVSP) and right ventricular hypertrophy index (RVHI)

RVSP equals to pulmonary artery systolic pressure (PASP) when the right ventricular outflow obstruction is absent according to the modified Bernoulli equation. RVSP was measured by inserting an eight-gauge needle with high-fidelity pressure transducer to right ventricle. The value of RVSP was recorded and analyzed by Power Lab Data Acquisition and Analysis System (PL 3504, AD Instruments, Australia). RVHI is identical to right ventricle over the sum of left ventricle plus septum (RV/LV + S) according to the Fulton index measurement.

2.9. Hydroxyproline assay (HYP) assay

HYP content of lung tissue was measured by a HYP kit (NBP2-59747, Novus Biologicals, Littleton, CO, USA) according to manufacturer's instructions. Approximately 20 mg of lung tissue was applied to calculate the HYP content.

2.10. Bronchoalveolar lavage fluid (BALF)

The collection of BALF refers to our previous study[22]. Briefly, after mechanical ventilation, we lavaged the lung through tracheal cannula with 0.9% saline 0.4 mL for three times and collected the lavage fluid. Samples were centrifuged at 1000 r/min (Eppendorf, Centrifuge 5424R) for 5 min at 4 °C and then the supernatant of BALF was stored at −80 °C waiting for testing.

2.11. Quantitative polymerase chain reaction (qPCR)

RNA was isolated with TRIzol reagent (Invitrogen, Carlsbad, CA, USA) according to the manufacture's procedures. DNA was synthesized by the Tiangen reverse transcription kit (KR103, Tiangen Biotechnology, Beijing, China). The mRNA levels were quantitated by using SYBR Green I Q-PCR kit with Bio-Rad IQ5 system (Bio-Rad, Hercules, CA, USA) and normalized to β-actin expression. Additional information about all the primers in this study were listed in the Supporting Information Table S1.

2.12. Western blot

Fresh tissue or cells were lysed with modified Radio Immunoprecipitation Assay (RIPA, P0013B, Beyotime, China) plus protease and phosphatase inhibitor cocktail (5872S, Cell Signaling Technology, MA, USA). For Western blot assay, tissue and cell protein (10 μg) were subjected to electrophoresis in 8%−15% SDS-polyacrylamide gradient gels and immunoblotted with the indicated antibodies. All the images were analyzed using Image J software (Image J 1.53a, National Institutes of Health, USA). See the Supporting Information Table S2 for all the antibodies in this study.

2.13. Enzyme-linked immunosorbent assay (ELISA)

The protein levels of IL-1β and IL-6 in cell supernatant and BALF were detected by enzyme-linked immunosorbent assay (ELISA) kit according to the instructions of the kit. See the Supporting Information Table S3 for specific kit information.

2.14. Lactate dehydrogenase (LDH) assay

LDH quantitative enzyme activity was detected by the LDH Assay kit (Abcam, ab102526, USA). We strictly followed the instructions, then measured the OD_{450} value, and finally calculated the amount of LDH according to the standard curve.

2.15. Microscopy imaging of pyroptosis

Peritoneal macrophages were fixed with 2.5% glutaraldehyde overnight, and then washed with PBS for three times. Cells were dehydrated by a grade series of ethanol (30%, 50%, 70%, 95%, and 100%) and dried with tertiary butanol. Specimens were sputter coated with gold-palladium for imaging. Pyroptotic morphology of macrophages was observed with a field-emmission scanning electron microscope (SEM, HITACHI SU8010, Japan).

To monitor the process of pyroptosis, we took photos of peritoneal macrophages plated onto 12-well plate bottom (Nest) for 8 h continuously by time-lapse phase contrast microscope (EVOS Evos FL Auto 2, Thermo Fisher Scientific, USA). We set an interval of 15 min in the first hour and an interval of 30 min in the last 7 h.

Propidium iodide (PI; 5 ng/mL) was added to the buffer for monitoring cell membrane integrity. Static images of pyroptotic cells were captured using a Nikon Eclipse Ti inverted microscope with a Nikon DS-Ri2 camera (Nikon, Tokyo, Japan). These pictures were analyzed using Image J software.

2.16. Statistical analysis

Data statistical analysis was performed using Prism 8.0 software (GraphPad Software, Inc.). Values were shown as mean ± standard error of the mean (SE). The Student-Newan-Keuls test was utilized between two groups and comparison between multiple groups with two variables was evaluated by two-way ANOVA. For all statistical methods, $P < 0.05$ were considered significance.

3. Results

3.1. GSDMD is upregulated in macrophages of human and murine silicosis lungs

In order to determine the relevant cell types and their specific patterns of pyroptosis-associated gene expression, we conducted

scRNA-seq-based analyses of silicosis lung tissue sampled from silicosis lung transplant patients and silicosis mouse models established by intratracheal administration of silica suspension (Fig. 1A). In silicosis patients, we identified 15 different cell populations (Fig. 1B). Since caspase-4/5/11 and caspase-1 have been previously established as upstream initiators of pyroptosis, we hypothesized that these factors would be activated in silica-induced pyroptotic cells. Supporting this hypothesis, we found that caspase-1, caspase-4/5, and *GSDMD* were mainly expressed in macrophages and monocytes at basal (Fig. 1C). Moreover, *GSDMD* (Supporting Information Fig. S1A), caspase-1 (Fig. S1B), and caspase-4 (Fig. S1C) expression were markedly increased in silicosis lung macrophages compared with those of the donor controls. In contrast, monocytes exhibited no significant alterations in *GSDMD* and caspase-4, except remarkably up-regulated trend in caspase-1. In light of these results, we selected macrophages as the focus of subsequent experiments.

scRNA-seq of murine silicosis and control lung tissue revealed 16 distinct cell populations (Fig. 1D). Among these cell types, macrophage and dendritic cell (DC) expressed the highest levels of caspase-11, caspase-1, and *Gsdmd* (Fig. 1E). This up-regulation of *Gsdmd* in macrophages and DCs were clearly detectable in samples from silicosis mice, compared with controls (Fig. S1D), whereas caspase-1 (Fig. S1E), the upstream molecules of *Gsdmd*, only increased in macrophages. As for caspase-11, it is down-regulated both in macrophages and DCs (Fig. S1F). Hence, we focused on macrophages rather than DCs as the prime candidates for activated pyroptosis in murine silicosis lung tissue.

In order to verify these RNA-seq data, we used IF staining of GSDMD and CD68 to further confirm that these pyroptosis-associated markers were expressed in macrophages of silicosis patients (Fig. 1F) and silicosis mice (Fig. 1G). Additionally, other effector cells, including epithelial cells (Fig. S1G) and fibroblasts (Fig. S1H), were also verified by IF staining to express low levels
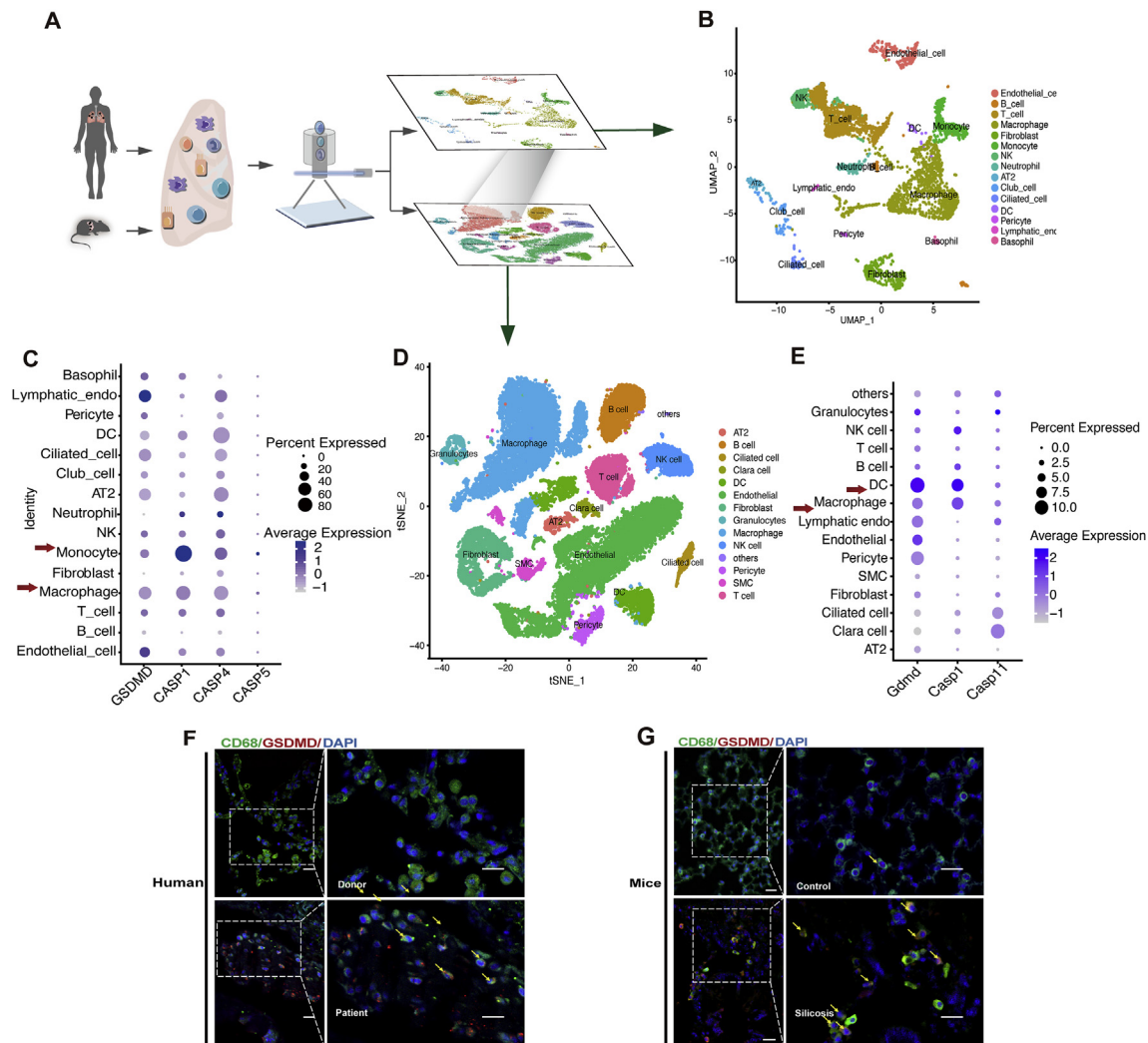

Figure 1 Up-regulated GSDMD-dependent pyroptosis in pulmonary macrophages of silicosis lungs from human and mice. (A) scRNA-seq of healthy and silicosis lung tissue from human lung transplant patients and donors as well as control and silicosis C57BL/6J mouse models. (B) Cell cluster analysis in silicosis patient lung tissue. (C) mRNA expression levels of *GSDMD*, *CASP1*, *CASP4*, and *CASP5* in different cell types of silicosis patient lung tissue. (D) Cell clusters in lung tissue of silicosis mice. (E) mRNA expression levels of *Gsdmd*, *Casp1*, and *Casp11* in different cell types in lung tissue of silicosis mice. (F, G) IF staining of macrophage marker CD68 (green), GSDMD (red), and DAPI (blue) in lung sections from human silicosis patients and silicosis mice. Dashed boxes show magnified field of view. Arrowheads indicate the colocalization of CD68 and GSDMD. Scale bar, 10 μm (short) and 5 μm (long).

of GSDMD. Taken together, these findings confirmed that pyroptosis actively occurred in macrophages of both human and murine silicosis lung tissue.

3.2. Silica induces pyroptosis-associated morphological changes, cell damage, IL-1β release, elevated LDH and GSDMD^{NT} in macrophages

Recently, the debate whether inflammatory caspases in macrophages could be activated without pre-stimulus is heating up. Classically, pyroptosis in macrophages usually requires LPS priming[23], such as pyroptotic positive control induced by LPS + Nig. However, some study provided proof that macrophages without pretreatment were still available for the activation of inflammasome[26]. We therefore set groups treated with silica alone and LPS + silica to investigate the pathophysiologic features and the underlying mechanisms of silica-induced pyroptosis.

The morphological features associated with pyroptosis have been widely reported to include plasma membrane rupture, formation of pyroptotic bodies, cellular swelling, and chromatin condensation[23]. In order to observe these morphological features of pyroptosis in silicosis lung tissue, and thereby distinguish pyroptosis from other programmed cell death modalities, we utilized phase contrast microscopy and SEM.

We found that the ultrastructures of PBS and LPS-pretreated macrophages exhibited similar morphology, whereas the silica and LPS + silica groups produced bubble-like cell protrusions, similar to those of the positive control (LPS + Nig) (Fig. 2A). Pyroptotic cells displayed swelling and cytoplasm flattening before rupture of the plasma membrane. Following membrane rupture, cytosolic LDH and high concentration of IL-1β could be observed in the extracellular space, and PI staining confirmed disruption of the cell membrane[27,28].

To further validate that pyroptosis was the relevant pathway, we quantified the concentration of IL-1β in cell supernatant (Fig. 2B) and mRNA level of Il-1β (Supporting Information Fig. S2A), in addition to performing LDH activity assays (Fig. 2C). We also observed that PI-positive cells increased over time after silica or LPS + silica treatment, indicating a decrease in cell viability and loss of membrane integrity (Fig. 2D). We found that Gsdmd mRNA levels were elevated in a time-dependent manner under silica stimulation and peaked at 3 h (Fig. S2B). Hence, we selected 3 h as an appropriate timepoint to detect pyroptosis and its related markers in the following experiments.

In order to detect the activation of pyroptosis, we measured protein and mRNA levels of full-length (GSDMD^{FL}) and cleaved GSDMD N terminal domain (GSDMD^{NT}), since GSDMD^{NT} mediates pyroptosis-associated pore formation. We found that mRNA (Fig. S2C) and protein levels of GSDMD (Fig. 2E and F) were elevated by treatment with silica and LPS + silica. Taken together, these results confirmed that silica could induce morphological changes, cell damage, release of effector cytokine IL-1β, and increasing levels of LDH and GSDMD^{NT} associated with GSDMD-dependent pyroptosis in macrophages.

3.3. GSDMD-induced pyroptosis is via both canonical and non-canonical pathways in silica-treated macrophages in vitro

To better understand the molecular mechanisms underlying silica-induced pyroptosis, we further investigated two upstream pathways previously reported to trigger GSDMD-induced pyroptosis, including the caspase-1 mediated inflammasome pathway (i.e., the canonical inflammasome pathway) and the caspase-4/5/11-mediated pathway (i.e., the non-canonical pathway)[29]. There are at least two hypotheses of how caspase-1 mediated canonical pathway is activated in macrophages: the indirect two-step process and the direct one-step process. The former one requires both priming signal and the subsequent activating signal, however, the later one triggers caspase-1 without primed stimulus. Classically, in the canonical inflammasome pathway, activation of NOD-like receptor family, pyrin domain containing 3 (NLRP3) inflammasome requires both priming and activating steps. Priming is usually mediated by the Toll-like receptor 4 (TLR4)−myeloid differentiation factor 88 (MyD88) pathway[30], whereas activating signals promote NLRP3, apoptosis associated speck-like protein containing a CARD (ASC), and pro-caspase-1 to assemble the NLRP3 inflammasome[30]. Upon inflammasome activation, pro-caspase-1 is cleaved to form mature caspase-1, which in turn mediates cleavage of GSDMD^{FL} into GSDMD^{NT} and maturation of pro-IL-1β and pro-IL-18 into IL-1β and IL-18, respectively. In contrast to the well-documented "two-hit" model, some studies found that some silica-treated macrophages, like THP-1, do not always require LPS priming to trigger the NLRP3 inflammasome and the subsequent caspase-1[26,31]. Similarly, caspase-11 can be triggered directly to induce GSDMD-dependent pyroptosis. First, we detected essential components of canonical inflammasome pathway following silica and LPS + silica stimulation in primary macrophages, depicting an increase in the mRNA and protein levels of caspase-1 (Fig. 3A, D, and E), NLRP3 (Fig. 3B, D, and F), TLR4 (Fig. 3D and F; Supporting Information Fig. S3A), and MyD88 (Fig. 3D and F; Fig. S3B), whereas no significant alteration in ASC (Fig. 3D and F; Fig. S3C) in silica-triggered macrophages. With regards to non-canonical pathway, it is observed that caspase-11 mRNA (Fig. 3C) and protein (Fig. 3D and G) levels were also up-regulated in silica and LPS + silica macrophages. Interestingly, our data supported that both pretreated with and without LPS, silica alone was capable of inducing activation of NLRP3 inflammasome and pyroptosis.

Furthermore, we applied caspase-1 inhibitor Beln and caspase-11 inhibitor Wede to further verify whether GSDMD-induced pyroptosis is mediated by the canonical and/or non-canonical pathways. At first, we validated that Beln and Wede inhibited the functional caspase-1 and caspase-11 in a dose-dependent manner, respectively (Fig. S3D and E). Then, we pre-treated cells with three different doses of Beln and Wede, respectively, and then exposed the primary macrophages to silica before detecting GSDMD^{NT} levels by Western blot. The results showed that both Beln and Wede inhibited the expression of GSDMD^{NT} in a dose-dependent manner (Fig. 3H and I). Moreover, the combined intervention with Beln and Wede was superior to the monotherapy of either Beln or Wede to suppress the vast majority of GSDMD expression (Fig. 3J), which suggested that pyroptosis is indeed mediated by these two pathways in macrophages treated with silica.

3.4. Silica induces GSDMD-dependent pyroptosis in lung tissue of silicosis mice and patients in vivo

In light of verification that GSDMD-dependent pyroptosis is involved in macrophages treated with silica in vitro, we next detected pyroptosis-associated events in lung tissue of silicosis patients and mice in vivo. We first used C57BL/6J mice to construct a murine model of silicosis, as previously described[22], and found that silicosis mice had remarkably enhanced lung
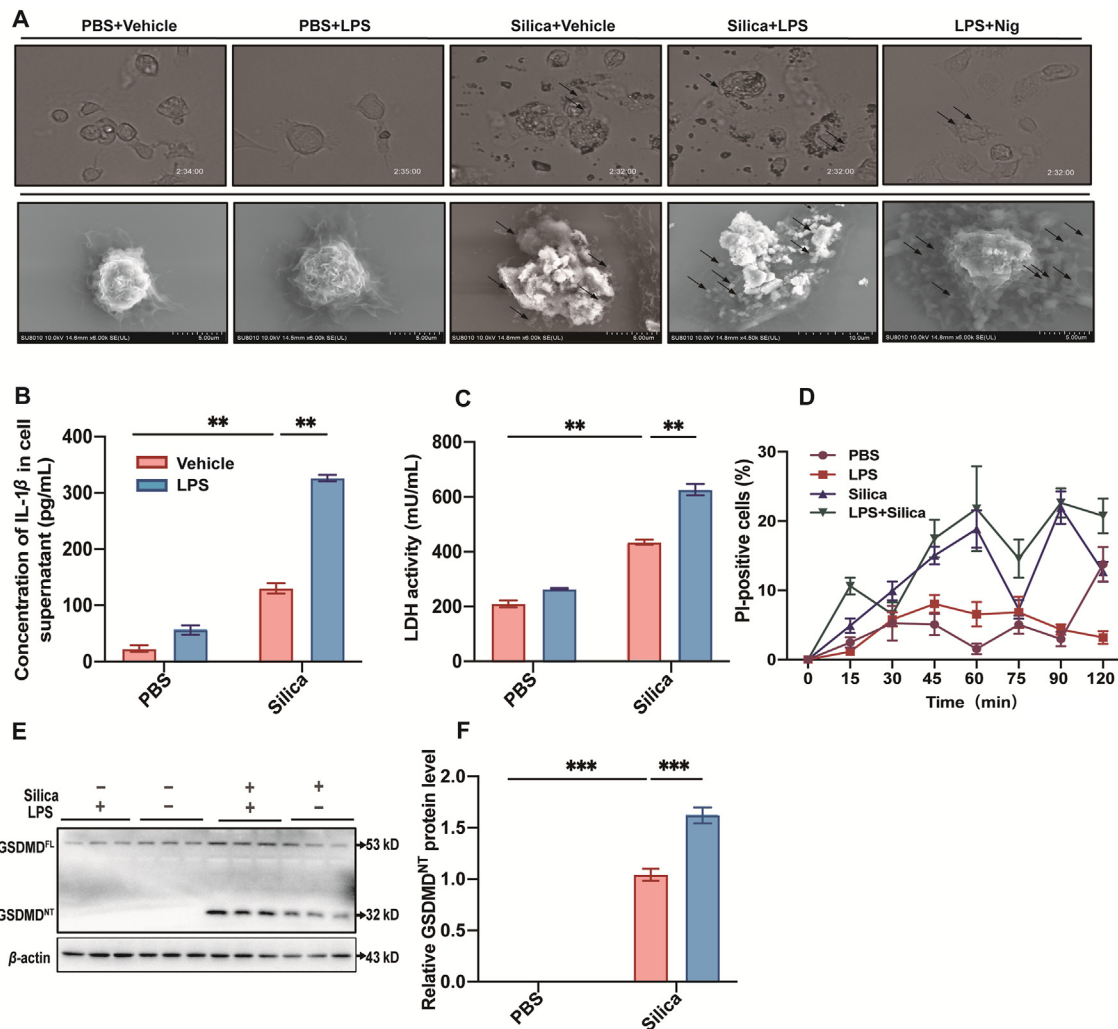
Figure 2 Silica induces GSDMD-dependent pyroptosis in macrophages. (A) Cell morphology was visualized by phase contrast microscope (top) and SEM (bottom). The arrows indicate bubbling of pyroptotic cells. (B) Concentration of IL-1β and (C) activity of LDH in cell supernatant. (D) Cell viability was monitored by PI detection for 120 min. (E) Western blot of GSDMD^{FL} and GSDMD^{NT}. (F) The statistical analysis of band densities in E. The data are reported as the mean $\pm$ SE. All experiments were repeated independently for three times ($n = 3$ per group). **$P < 0.01$, ***$P < 0.001$.

inflammation, indicated by the Szapiel Scores (Supporting Information Fig. S4A and B), significantly up-regulated mRNA levels of the pro-inflammatory cytokines *Il-1β* (Fig. 4I), *Il-6* (Fig. S4D), and *Tnf-α* (Fig. S4E). We also observed substantial progression of lung fibrosis indicated by Masson staining and significantly higher Fibrotic lesion Scores (Fig. S4A and C) as well as mRNA and protein levels of fibronectin-1 (FN-1) (Fig. S4F and H) and mRNA levels of collagen-I (*Col-I*) (Fig. S4G). Then, we employed IHC staining to observe GSDMD levels in murine silicosis lung tissue (Fig. 4A). Notably, we found that GSDMD levels were higher in the silicotic foci than in the control (PBS) group (Fig. 4B), indicating the occurrence of GSDMD-induced pyroptosis. Consistent with this result, mRNA (Fig. 4C−E) and protein (Fig. 4F and G) levels of pyroptosis markers (GSDMD, caspase-1, and caspase-11) were up-regulated in silicosis mice. In addition, IL-1β translational level in BALF (Fig. 4H), and *Il-1β* transcription level in murine silicosis lung tissue (Fig. 4I) were both elevated by silica treatment, suggesting that GSDMD-dependent pyroptosis likely contributes to inflammatory cytokine

release in silicosis. More importantly, detection of GSDMD levels by IHC in human silicosis lungs (Fig. 4J and K) revealed higher accumulation of this marker compared to that in donor lungs, which further supported the involvement of GSDMD-dependent pyroptosis in pulmonary silicosis macrophages observed in mouse model. Collectively, these findings revealed that GSDMD-driven pyroptosis is closely related to the onset and progression of silicosis.

3.5. *Gsdmd*⁻/⁻ mice are resistant to developing silicosis

To further verify the critical role of pyroptosis in the pathogenesis of silicosis, mouse models were established in *Gsdmd*⁻/⁻ mice and WT mice (Fig. 5A). Compared with the silica-exposed WT mice, lung resistance and compliance, which are specifically associated with pulmonary fibrosis, were both improved in *Gsdmd*⁻/⁻ mice, indicated by Cchord (Fig. 5B), RI (Fig. 5C), and Cdyn (Supporting Information Fig. S5B), whereas pulmonary ventilation function, indicated by IC (Fig. S5A), was not significantly increased in
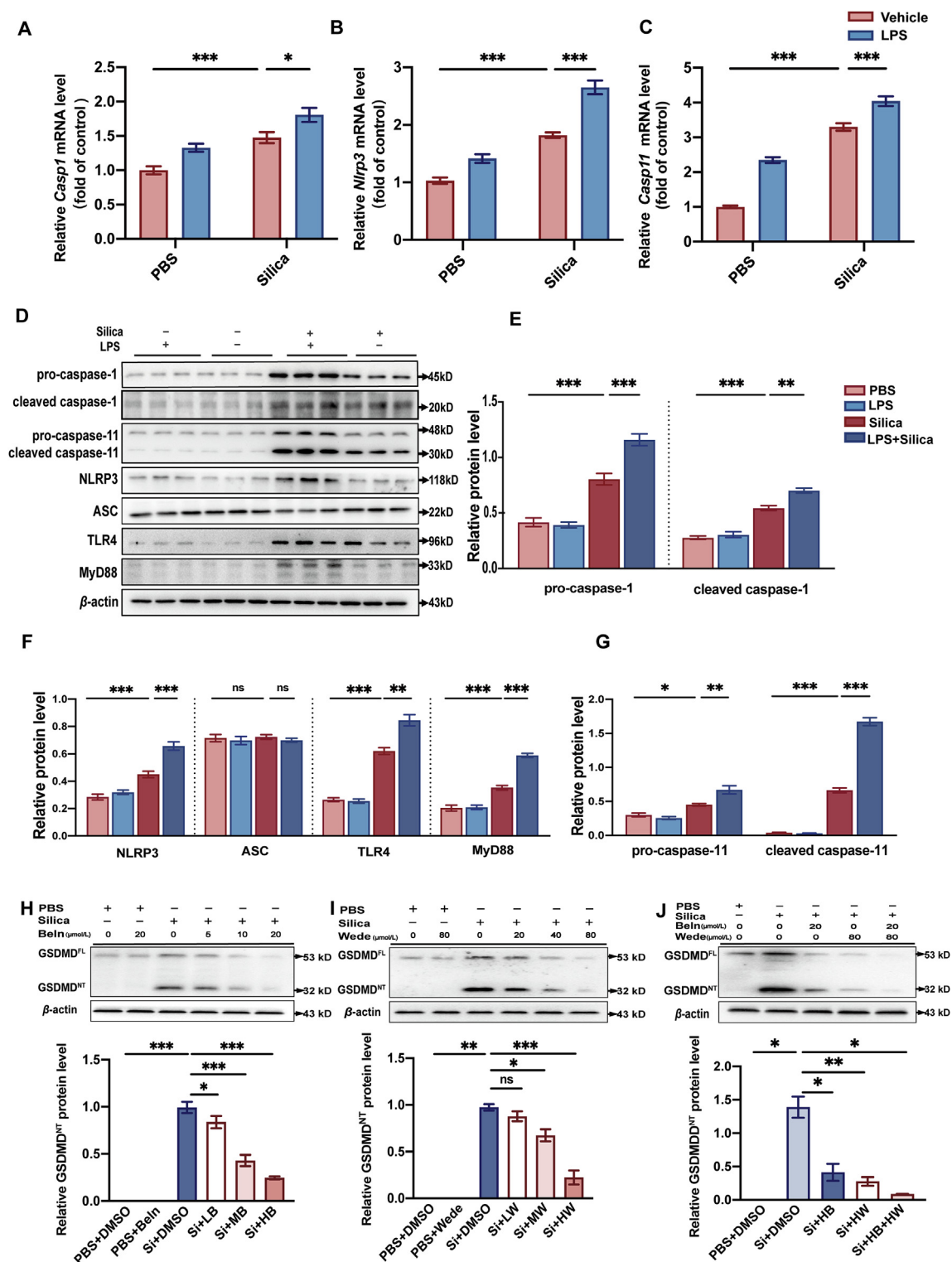
Figure 3 GSDMD-induced pyroptosis is mediated by canonical and non-canonical pathways in macrophages treated with silica. (A−C) *Casp1*, *Nlrp3*, and *Casp11* mRNA levels in LPS- or vehicle-activated macrophages exposed to silica or not. (D) Western blots of pro-caspase-1, cleaved caspase-1, pro-caspase-11, cleaved caspase-11, NLRP3, ASC, TLR4, and MyD88 in macrophages under same treatments as A−C. (E−G) Statistical analysis of protein levels from Western blots in Fig. 3D. (H) Western blots of GSDMD in macrophages treated with different doses of caspase-1 inhibitor Beln (5, 10, and 20 μmol/L). The lower statistical graph indicates GSDMD^{NT} protein levels. (I) Western blots of GSDMD in macrophages treated with different doses of caspase-11 inhibitor Wede (20, 40, and 80 μmol/L). The lower statistical graph indicates GSDMD^{NT} protein levels. (J) Western blots of GSDMD in macrophages treated with high dose of Beln (20 μmol/L) and Wede (80 μmol/L). The lower statistical graph indicates GSDMD^{NT} protein levels. The data are reported as the mean ± SE. All experiments were repeated independently for three times ($n = 3$ per group). *$P < 0.05$, **$P < 0.01$, ***$P < 0.001$, and ns indicates not significant.
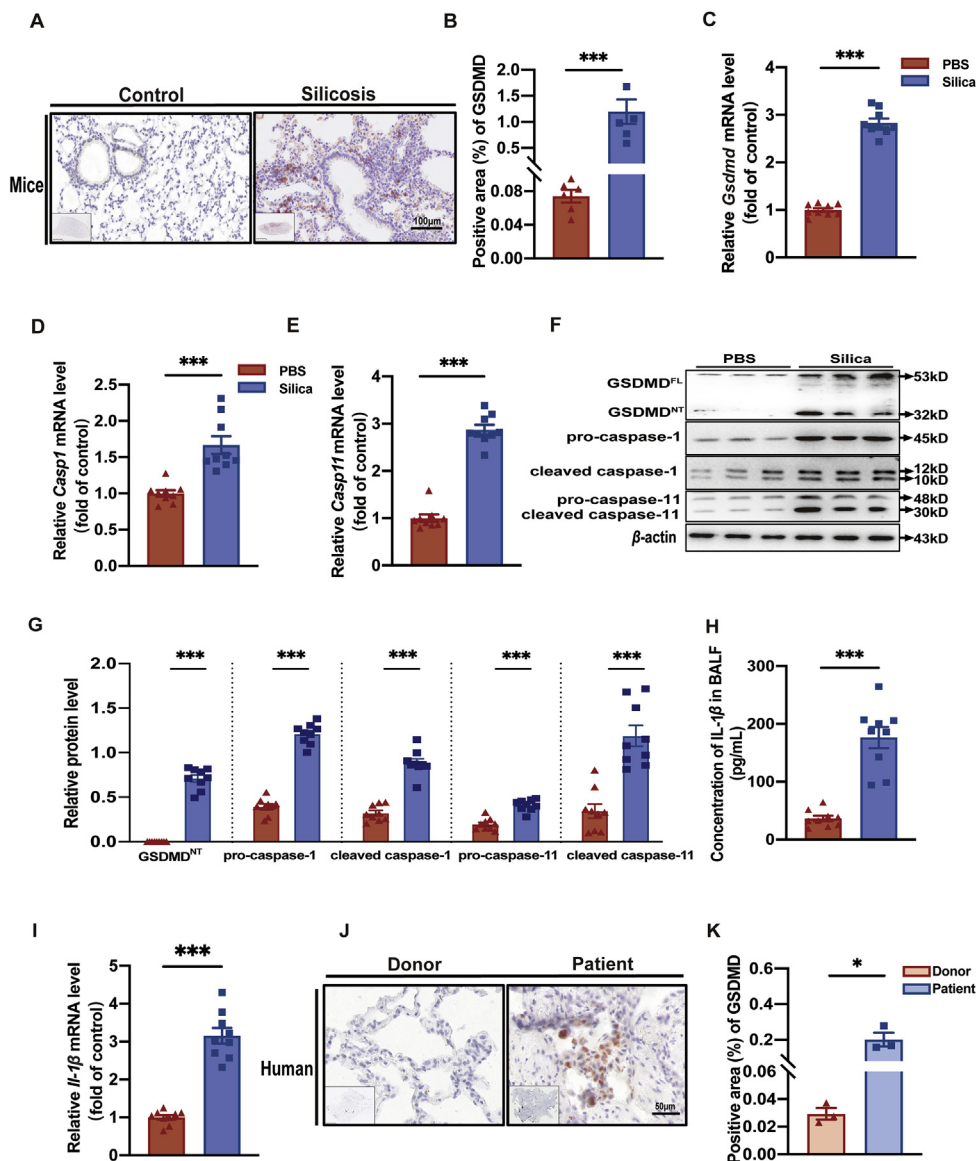
Figure 4 Silica induces GSDMD-dependent pyroptosis in mouse and human lungs. (A) GSDMD expression in silicosis or control lung tissue of mice by IHC. Scale bar, 100 μm. (B) Statistical analysis of GSDMD expression in images of A. (C−E) *Gsdmd*, *Casp1*, and *Casp11*, relative mRNA levels in lung tissue of silicosis and control mice. (F) Western blot detection of GSDMD^{FL}, GSDMD^{NT}, pro-caspase-1, cleaved caspase-1, pro-caspase-11, and cleaved caspase-11 in silicosis or control mouse lung tissue. (G) Statistical analysis of band densities from images in F. (H) IL-1β concentration in BALF from silicosis and control mice. (I) *Il-1β* relative mRNA levels in lung tissues of silicosis and control mice. The red and blue columns in B−E and G−I represent the PBS group and silica group, respectively. (J) GSDMD expression in silicosis and donor lung tissue of human patients by IHC. Scale bar, 100 μm for mice and 50 μm for human. (K) Statistical analysis of GSDMD-positive areas in images from J. The data are reported as the mean ± SE (*n* = 9 mice per group). *$P < 0.05$, ***$P < 0.001$.

silicosis. These lung function indicators demonstrated that *Gsdmd* deficiency was protective against silicosis development and progression. The extent of pulmonary hypertension and the subsequent right ventricular remodeling, indicated by RVSP (Fig. 5D) and RVHI (Fig. S5C), were decreased in silica-exposed *Gsdmd*$^{-/-}$ mice. These data suggested that *Gsdmd* deficiency exerted protective effects on cardiopulmonary function in silicosis mice. The diffuse alveolitis assessed by HE staining (Fig. 5E; Fig. S5D) and mRNA and protein levels of pro-inflammatory cytokines IL-1β (Fig. 5F and G) and IL-6 (Fig. S5E and F) were both down-regulated, suggesting *Gsdmd* knockout inhibited pulmonary inflammation during silicosis.

Masson staining (Fig. 5H; Fig. S5G) depicted that collagen deposition was decreased and silicotic nodule lesions reduced in size in silica-exposed *Gsdmd*$^{-/-}$ mice compared with control mice, confirmed by the hydroxyproline assay (Fig. 5I). Furthermore, mRNA level of *Col-I* (Fig. 5J) and mRNA (Fig. 5K) and protein (Fig. 5L; Fig. S5H) levels of FN-1, were lower in *Gsdmd*$^{-/-}$ mice, indicating that knocking out *Gsdmd* reduced the formation of silicotic nodules to suppress fibrosis. Collectively, *Gsdmd* gene deficiency resulted in a more anti-inflammatory and anti-fibrotic pulmonary microenvironment during silicosis, rendering mice more resistant to the silica stimulus.
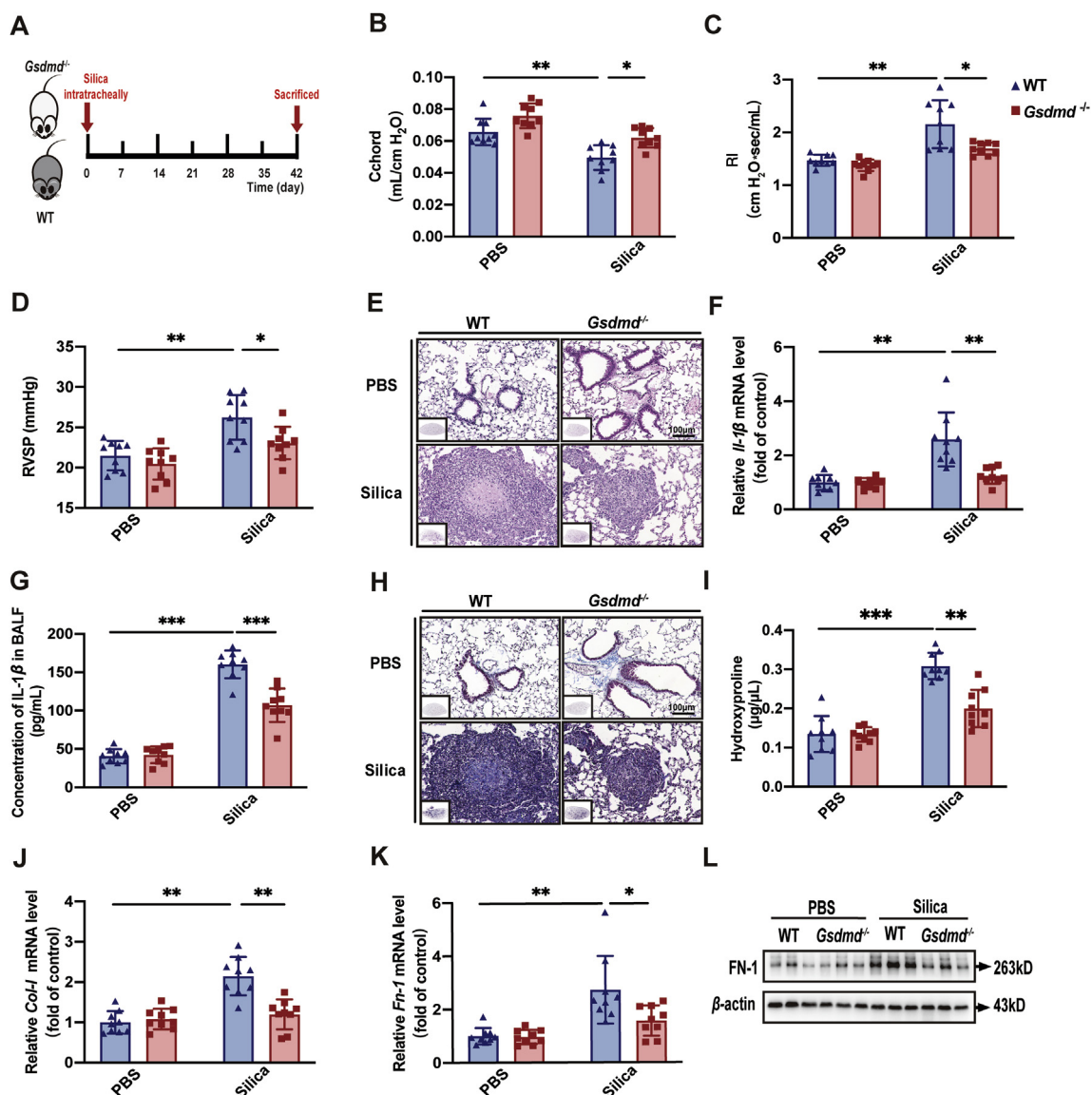
Figure 5 *Gsdmd*$^{-/-}$ mice are resistant to silicosis progression. (A) *Gsdmd*$^{-/-}$ and WT C57BL/6J mice were used to establish silicosis models by a single intratracheal silica administration and these mice were sacrificed at Day 42 after silica exposure. There were four groups (WT-PBS, WT-Si, *Gsdmd*$^{-/-}$-PBS, and *Gsdmd*$^{-/-}$-Si groups) with 9 mice per group. (B) Lung function test of Cchord and (C) RI of mice in different experimental groups. (D) RVSP of mice treated as in A. (E) Representative images of HE saining of lung sections from mice. (F) mRNA level of *Il-1β* in lung tissue from mice. (G) Concentration of IL-1β in BALF from mice. (H) Representative images of Masson saining of lung sections from mice. (I) Hydroxyproline assay of lung tissue from mice. (J) mRNA levels of *Col-I* and (K) *Fn-1* in lung tissue from mice. (L) Western blot of FN-1 in lung tissue from mice. The data are reported as mean ± SE (*n* = 9 mice per group). Significance for each figure: *$P < 0.05$, **$P < 0.01$, ***$P < 0.001$.

4. Discussion

In this work, we found that GSDMD-induced pyroptosis is involved in both human and murine silicosis. scRNA-seq of lung tissue from silicosis lung transplant patients and mice indicated that GSDMD-dependent pyroptosis (triggered by caspase-1 and caspase-4/5/11) occurred in the macrophages of this tissue. Further, *in vivo* and *in vitro* results verified the findings of scRNA-seq, which indicated the active occurrence of pyroptosis in silicosis-related macrophages, through observation of pyroptosis-associated alterations in cell morphology and biochemical markers, including IL-1β release, LDH activity, and PI staining of compromised cells. Since caspase-1 and caspase-4/5/11-dependent cleavage of GSDMD are

primarily responsible for eliciting pyroptosis[15], investigation of canonical and non-canonical pathways revealed that both are active during silicosis. We therefore proposed that macrophage in silicosis lung underwent GSDMD-driven pyroptosis which was mediated by both caspase-1 and caspase-11 in silicosis. Importantly, our results showed that knocking out *Gsdmd* markedly attenuated silicosis *in vivo*. Collectively, based on our study, we could demonstrate that GSDMD-driven pyroptosis indeed occurs in the development of silicosis and inhibition of this type of cell death could ameliorate silicosis, underscoring the importance of this process as new drug target for silicosis.

Pyroptosis has been described as a potent regulator of cytokine release and cell death in various inflammatory and

fibrogenetic lung diseases[14,32]. Recent work has shown that caspase-4/5/11-induced pyroptosis in human and murine macrophages is associated with allergic airway inflammation, which has important implications for the pathogenesis of asthma[33]. Further, a loss-of-function mutation in the gasdermin-encoding gene has been closely linked to reducing risk of asthma, implicating pyroptosis as an underlying basis of asthma rather than secondary inflammation[19,34]. Similarly, suppression of pyroptosis alleviates acute lung injury (ALI)/ARDS by limiting the disruption of effector cells and consequently reducing IL-1β release[35-37]. For example, miRNA-495 was shown to attenuate LPS-induced lung injury by negatively regulating NLRP3 inflammasome-mediated pyroptosis in alveolar macrophages[35]. In addition, a recent study demonstrated that lycorine, an alkaloid extract of Amaryllidaceae plants, can ameliorate bleomycin-induced pulmonary fibrosis by inhibiting pyroptosis and the assembly of the NLRP3 inflammasome, suggesting that attenuation of early pyroptotic hyper inflammation contributes to reversing late-stage fibrosis[17]. In line with these published results, our data demonstrated that silicosis macrophages in mice also exhibit upregulation of GSDMD-induced pyroptosis. More importantly, inhibition of this pyroptosis by knocking out Gsdmd gene could attenuate silicosis progression in mice. As discussed above, pyroptosis in effector cells can thus frequently lead to detrimental consequences associated with various lung diseases, and our study firstly proved that suppression of GSDMD-induced pyroptosis impedes silicosis progression.

Recently, GSDMD[NT] was identified as a predominant mediator of pyroptosis, indicating its viability as a promising therapeutic target for inflammatory diseases[15,37]. Researchers have identified several small molecule inhibitors that inactivate GSDMD[NT] to block pyroptosis, including necrosulfonamide (NSA), disulfiram, Bay 11-7082, and LDC7559[38-40]. Among these, both NSA and disulfiram target the Cys191/192 residue in GSDMD that is indispensable to pore formation in plasma membrane. These two inhibitors exhibited considerable efficacy against pyroptosis by blocking IL-1β release and prolonging the survival of pyroptotic monocytes/macrophages during sepsis[38-40]. Unfortunately, both NSA and disulfiram still block other targets, indicating that their activity is not pyroptosis-specific. Hence, there is a significant need to research and develop the specific GSDMD inhibitor to treat these inflammatory diseases. Since it is a lack of effective GSDMD inhibitor, we selected genetic deletion Gsdmd to treat silicosis, harvesting good therapeutic effects. Our findings suggested that inhibition of GSDMD-dependent pyroptosis may be a viable clinical therapeutic strategy for silica-induced pulmonary inflammation and fibrosis.

At last, given the low availability and hence small sample size of transplanted silicosis lungs in this study, the statistical power necessary for reliable correlations is extremely limited. Future study will include more samples from silicosis patients, and in particular, BALF samples will be used to further verify the occurrence of GSDMD-dependent pyroptosis in macrophages.

5. Conclusions

Our work verified active occurrence of GSDMD-induced pyroptosis in silicosis macrophages as well as in silicosis patients and mice. In silicosis, GSDMD-induced pyroptosis is mediated by canonical (caspase-1) and non-canonical (caspase-4/5/11) signaling pathways *in vitro* and *in vivo*. Inhibition of pyroptosis exhibited favorable therapeutic outcomes *in vivo*, suggesting GSDMD may be a promising target for developing anti-silicosis drugs. Hence, expanding the availability of specific and effective drugs for inhibiting GSDMD should be a research priority for silicosis treatment. Moreover, GSDMD-driven pyroptosis and the concurrent secretion of alarmins that together are termed damage-associated molecular patterns (DAMPs), usually serve as key drivers of inflammatory and immune cell death[37]. Further investigation should therefore focus on the identity and function of specific DAMPs, beyond IL-1β, in the silicosis-related pyroptosis milieu.

In summary, we provide the first report to our knowledge of the presence of GSDMD-induced pyroptosis in macrophages of silicosis lung tissue and showed preliminary evidence that capsase-1 and caspase-4/5/11 mediate its activation and mice knocking out Gsdmd are resistant to silicosis development and progression. This discovery provides novel insights for a comprehensive understanding of silicosis and suggests promising targets for its treatment.

Author contributions

Jing Wang, Chen Wang, and Xinri Zhang designed and supervised the whole project. Meiyue Song and Jiaxin Wang drafted the manuscript with contribution from all authors. Jing Wang and Peiran Yang revised and reviewed the manuscript. Meiyue Song and Baicun Li constructed the experimental silicosis model. Meiyue Song, Ying Liu, Tianhui Fan, Zhaoguo Li, and Xianmei Qi contributed to harvesting animals and lung functional test. Meiyue Song, Jiaxin Wang, Youliang Sun, Xiaona Li, and Yuan Liu performed all the pathological and biomolecular experiments. Junling Pang and Yitian Zhou analyzed the single-cell RNA sequencing data. We thank Professor Feng Shao (National Institute of Biological Sciences, Beijing, China) for generously providing the Gsdmd knockout mice. All authors approved of the final version of the manuscript and are accountable for all aspects of this work. Meiyue Song and Jiaxin Wang contributed equally to this article.

Conflicts of interest

The authors declared no conflict of interest in this present study.

Appendix A. Supporting information

Supporting data to this article can be found online at https://doi.org/10.1016/j.apsb.2021.10.006.

References

1. Leung CC, Yu ITS, Chen W. Silicosis. *Lancet* 2012;**379**:2008−18.
2. Perlman DM, Maier LA. Occupational lung disease. *Med Clin North Am* 2019;**103**:535−48.
3. Rushton L. The global burden of occupational disease. *Curr Environ Health Rep* 2017;**4**:340−8.
4. Barnes H, Goh NSL, Leong TL, Hoy R. Silica-associated lung disease: an old-world exposure in modern industries. *Respirology* 2019;**24**:1165−75.
5. Hamilton RF, Thakur SA, Holian A. Silica binding and toxicity in alveolar macrophages. *Free Radic Biol Med* 2008;**44**:1246−58.
6. Guo J, Gu N, Chen J, Shi T, Zhou Y, Rong Y, et al. Neutralization of interleukin-1 beta attenuates silica-induced lung inflammation and fibrosis in C57BL/6 mice. *Arch Toxicol* 2013;**87**:1963−73.
7. Hoffman HM, Wanderer AA. Inflammasome and IL-1β-mediated disorders. *Curr Allergy Asthma Rep* 2010;**10**:229−35.
8. Batista SJ, Still KM, Johanson D, Thompson JA, O'Brien CA, Lukens JR, et al. Gasdermin-D-dependent IL-1α release from microglia promotes protective immunity during chronic *Toxoplasma gondii* infection. *Nat Commun* 2020;**11**:3687.
9. Evavold CL, Ruan J, Tan Y, Xia S, Wu H, Kagan JC. The Pore-forming protein gasdermin D regulates interleukin-1 secretion from living macrophages. *Immunity* 2018;**48**:35−44.
10. He WT, Wan H, Hu L, Chen P, Wang X, Huang Z, et al. Gasdermin D is an executor of pyroptosis and required for interleukin-1β secretion. *Cell Res* 2015;**25**:1285−98.
11. Luan J, Chen W, Fan J, Wang S, Zhang X, Zai W, et al. GSDMD membrane pore is critical for IL-1β release and antagonizing IL-1β by hepatocyte-specific nanobiologics is a promising therapeutics for murine alcoholic steatohepatitis. *Biomaterials* 2020;**227**:119570.
12. Xia S, Zhang Z, Magupalli VG, Pablo JL, Dong Y, Vora SM, et al. Gasdermin D pore structure reveals preferential release of mature interleukin-1. *Nature* 2021;**593**:607−11.
13. Shi J, Gao W, Shao F. Pyroptosis: gasdermin-mediated programmed necrotic cell death. *Trends Biochem Sci* 2017;**42**:245−54.
14. Sauler M, Bazan IS, Lee PJ. Cell death in the lung: the apoptosis-necroptosis axis. *Annu Rev Physiol* 2019;**81**:375−402.
15. Broz P, Pelegrín P, Shao F. The gasdermins, a protein family executing cell death and inflammation. *Nat Rev Immunol* 2020;**20**:143−57.
16. Orning P, Lien E, Fitzgerald KA. Gasdermins and their role in immunity and inflammation. *J Exp Med* 2019;**216**:2453−65.
17. Liang Q, Cai W, Zhao Y, Xu H, Tang H, Chen D, et al. Lycorine ameliorates bleomycin-induced pulmonary fibrosis *via* inhibiting NLRP3 inflammasome activation and pyroptosis. *Pharmacol Res* 2020;**158**:104884.
18. Kim RY, Pinkerton JW, Essilfie AT, Robertson AAB, Baines KJ, Brown AC, et al. Role for NLRP3 inflammasome-mediated, IL-1β-dependent responses in severe, steroid-resistant asthma. *Am J Respir Crit Care Med* 2017;**196**:283−97.
19. Panganiban RA, Sun M, Dahlin A, Park H-R, Kan M, Himes BE, et al. A functional splice variant associated with decreased asthma risk abolishes the ability of gasdermin B to induce epithelial cell pyroptosis. *J Allergy Clin Immunol* 2018;**142**:1469−78.e2.
20. Kovarova M, Hesker PR, Jania L, Nguyen M, Snouwaert JN, Xiang Z, et al. NLRP1-dependent pyroptosis leads to acute lung injury and morbidity in mice. *J Immunol* 2012;**189**:2006−16.
21. Yang J, Zhao Y, Zhang P, Li Y, Yang Y, Yang Y, et al. Hemorrhagic shock primes for lung vascular endothelial cell pyroptosis: role in pulmonary inflammation following LPS. *Cell Death Dis* 2016;**7**:e2363.
22. Cao Z, Song M, Liu Y, Pang J, Li Z, Qi X, et al. A novel pathophysiological classification of silicosis models provides some new insights into the progression of the disease. *Ecotoxicol Environ Saf* 2020;**202**:110834.
23. Chen X, He WT, Hu L, Li J, Fang Y, Wang X, et al. Pyroptosis is driven by non-selective gasdermin-D pore and its morphology is different from MLKL channel-mediated necroptosis. *Cell Res* 2016;**26**:1007−20.
24. Szapiel SV, Elson NA, Fulmer JD, Hunninghake GW, Crystal RG. Bleomycin-induced interstitial pulmonary disease in the nude, athymic mouse. *Am Rev Respir Dis* 1979;**120**:893−9.
25. King EJ. Silicosis. *Lect Sci Basis Med* 1952;**2**:108−38.
26. Peeters PM, Perkins TN, Wouters EFM, Mossman BT, Reynaert NL. Silica induces NLRP3 inflammasome activation in human lung epithelial cells. *Part Fibre Toxicol* 2013;**10**:3.
27. Davis BK, Wen H, Ting JPY. The inflammasome NLRs in immunity, inflammation, and associated diseases. *Annu Rev Immunol* 2011;**29**:707−35.
28. Latz E, Xiao TS, Stutz A. Activation and regulation of the inflammasomes. *Nat Rev Immunol* 2013;**13**:397−411.
29. Lu F, Lan Z, Xin Z, He C, Guo Z, Xia X, et al. Emerging insights into molecular mechanisms underlying pyroptosis and functions of inflammasomes in diseases. *J Cell Physiol* 2020;**235**:3207−21.
30. Elliott EI, Sutterwala FS. Initiation and perpetuation of NLRP3 inflammasome activation and assembly. *Immunol Rev* 2015;**265**:35−52.
31. Peeters PM, Eurlings IMJ, Perkins TN, Wouters EF, Schins RPF, Borm PJA, et al. Silica-induced NLRP3 inflammasome activation *in vitro* and in rat lungs. *Part Fibre Toxicol* 2014;**11**:58.
32. Liang F, Zhang F, Zhang L, Wei W. The advances in pyroptosis initiated by inflammasome in inflammatory and immune diseases. *Inflamm Res* 2020;**69**:159−66.
33. Zasłona Z, Flis E, Wilk MM, Carroll RG, Palsson-McDermott EM, Hughes MM, et al. Caspase-11 promotes allergic airway inflammation. *Nat Commun* 2020;**11**:1055.
34. Chao KL, Kulakova L, Herzberg O. Gene polymorphism linked to increased asthma and IBD risk alters gasdermin-B structure, a sulfatide and phosphoinositide binding protein. *Proc Natl Acad Sci U S A* 2017;**114**:E1128−37.
35. Ying Y, Mao Y, Yao M. NLRP3 inflammasome activation by microRNA-495 promoter methylation may contribute to the progression of acute lung injury. *Mol Ther Nucleic Acids* 2019;**18**:801−14.
36. Cheng KT, Xiong S, Ye Z, Hong Z, Di A, Tsang KM, et al. Caspase-11-mediated endothelial pyroptosis underlies endotoxemia-induced lung injury. *J Clin Invest* 2017;**127**:4124−35.
37. Galluzzi L, Vitale I, Aaronson SA, Abrams JM, Adam D, Agostinis P, et al. Molecular mechanisms of cell death: recommendations of the nomenclature committee on cell death 2018. *Cell Death Differ* 2018;**25**:486−541.
38. Rathkey JK, Zhao J, Liu Z, Chen Y, Yang J, Kondolf HC, et al. Chemical disruption of the pyroptotic pore-forming protein gasdermin D inhibits inflammatory cell death and sepsis. *Sci Immunol* 2018;**3**:eaat2738.
39. Sollberger G, Choidas A, Burn GL, Habenberger P, Di Lucrezia R, Kordes S, et al. Gasdermin D plays a vital role in the generation of neutrophil extracellular traps. *Sci Immunol* 2018;**3**:eaar6689.
40. Pandeya A, Li L, Li Z, Wei Y. Gasdermin D (GSDMD) as a new target for the treatment of infection. *Medchemcomm* 2019;**10**:660−7.